Journal of Probability and Statistical Science
24(2), 1-15Aug. 2026

A Ridge-Penalised Fourier Autoregressive Framework for High-Dimensional Periodic Time Series Dataset

Okolie, F. A.
Department of Mathematical Sciences
Ajayi Crowther University, Nigeria

Taiwo, A. I.
Department of Statistics
Olabisi Onabanjo University, Nigeria

Olatayo, T. O.
Department of Statistics
Olabisi Onabanjo University, Nigeria

ABSTRACT

Time series associated with the seasonal climate are highly persistent with strong periodic behaviour making reliable statistical forecasting a challenge. Integrated autoregressive models on a conventional framework may fail to represent multifrequency seasonality. Fourier Autoregressive (FAR) models offer flexibility but may experience instability when the model complexity escalates in nature. The objective of this study is to improve forecast and parameter stability in the Fourier autoregressive framework by consideration of ridge penalisation. Using Nigeria's data on monthly rainfall and relative humidity from 2014 to 2024, the study creates and estimates classical FAR and ridge-penalised FAR models. Results from the ADF and KPSS tests on stationary indicate both series become stationary after first differencing. The identification of the model is done on the basis of information criteria and periodic correlation analysis. The out-of-sample Root Mean Square Error and Mean Absolute Percentage Error is used to evaluate the forecast performance. Fourier-based models help achieve far superior results than conventional ARIMA specifications, according to the empirical results. $FAR(4)$ reduces RMSE from 90.94 based on $ARIMA(1,1,1)$ to 73.72 when applied for rainfall, but ridge-penalised FAR further improves performance with lowest RMSE of 73.31. Further, MAPE goes down to 197.09 from 515.34. Similar improvements occur for relative humidity. The RMSE declines from 9.68 under $ARIMA(2,1,2)$ to 6.60 for $FAR(4)$, and further to 6.34 for $PFAR-Ridge$. Diagnostic findings validate well-mannered residuals with no remaining serial dependence. The research concludes that ridge penalisation improves the generalisation potential of Fourier autoregressive models, thereby resulting in a robust and reliable framework for seasonal climatic time series forecasting with strong periodic structures.

1. Introduction

The climate of a tropical region is hot and humid, with heavy rainfall throughout the year. Tropical regions are characterized by having mean monthly temperatures greater than 18 °C all the year round, just not as cold as frost all the time. However, there are huge variations in humidity and rainfall depending on the climate zone (The British Geographer, 2014). The equatorial climate receives a lot of rain throughout the year. On the other hand, the tropical wet-dry and monsoon climates see a significant seasonal change in the intensity and frequency of rainfall. Relative humidity (RH) determines how close the air is to saturation with water vapour. It is instrumental in biological processes, climate regulation, and energy redistribution in tropical regions (Borma, et al., 2022). Water vapour is the major greenhouse gas which warms the atmosphere through absorbing outgoing long-wave radiation and affecting the energy balance at the Earth's surface (El Zein & Chehayeb, 2015; Met Office, 2024).

The pattern of rainfall in the tropics is associated with humidity as a wet atmosphere creates the possibility of rainfall. Rainfall in tropical zones is more frequent and intense compared with temperate zones (Met Office, 2024). Rainfall is important for ecosystem productivity; in the tropics, rainfall recharges the forest profile to cut off a large portion of the terrestrial carbon and help reducing global warming (Zhou et al., 2023). At once, climate

Received April 6, 2026, in final form August 2026.
Okolie, F. A. (corresponding author) is affiliated with Department of Mathematical Sciences, Ajayi Crowther University, Nigeria
Email: fa.okolie@acu.edu.ng

change driven severe rainfall events are known to disrupt soil nutrients, the infrastructure of hydro-electricity and the economy at a regional level (Sartorius et al., 2024). According to Gevaudan (2021), precipitation events in tropical regions moderates sea-surface salinity in the Intertropical Convergence Zone.

In tropical developing countries, predominantly rain-fed agriculture important for economic livelihoods, modelling and forecasting of rainfall and relative humidity is important for climate monitoring, flood risk management, agricultural planning and sustainability of water-resource. The observed persistence and seasonality of tropical climate variables can be primarily attributed to monsoon and seasonal transitions that impact the cropping and water cycle (Jackson et al. 2025). Nonetheless, the presence of inadequate observation infrastructure and high climatic variability in a number of developing countries makes it difficult to make reliable forecasts. Therefore, it would be useful to develop robust statistical models that can use data to offer solutions to complex periodic problems (Makokha et al., 2025).

The classical time series models of autoregressive (AR) and autoregressive integrated moving average (ARIMA) are popular due to capturing temporal dependence. Nonetheless, complex seasonal or multi-frequency periodic structures needed for climate modelling is often poorly represented by these models. Seasonal ARIMA (SARIMA) models incorporate seasonality through set, periodic components. But, holding fixed this prior assumption may be too restrictive if periodicities evolve over time or multiple seasonal frequencies coexist. When excessive differencing or ad-hoc seasonal adjustment occurs, one may end up losing information, obtaining less interpretable outputs while the forecast may perform poorly; this may be aggravated with nonlinearity and noise.

Recent studies have pointed these out. According to Effrosynidis et al. (2023), after studying 68 variables at different temporal resolutions, and while ARIMA-type models are reasonably well-performing, regression-based approaches (regularised also) often outpredict classical time-series models across forecasting horizons. Accordingly, the study by Arumugam and Natarajan (2023) indicated that appropriate choice of ARIMA and SARIMA models yields good in-sample fit. However, the issues of parsimony, stationarity and over-fitness continued to exist. Most of these issues arise when modeling complex climatic datasets.

Harmonic expansions can be used to capture smooth seasonal and periodic dynamics through a Fourier-based modelling framework. Pure Fourier regression models are capable of representing periodicity, but ignore serial dependence, which gives rise to residual autocorrelation and limited forecasting ability FAR models have autoregressive dynamics and Fourier terms, which means the approach allows one to model both temporal dependence and seasonal structure. According to Taiwo et al., (2019) and Taiwo et al., (2020), application of FAR models on climatic variables, especially rainfall, preserves periodic patterns and generates stable forecasts (Taiwo et al., 2019; Taiwo et al., 2020). Nonetheless, as many harmonics or higher autoregressive order are included, the FAR models can become over-parameterised, leading to multicollinearity and overfitting (Papaioannou et al., 2022).

Regularisation offers a principled way of controlling model complexity to alleviate these issues. Coefficient magnitudes are shrunk, but harmonic components are not eliminated. This is good for numerical stability and generalisation performance, but most importantly helps retain the smooth seasonal structure. Ridge penalisation can mitigate multicollinearity-related instability relative to OLS and provide stable estimates in ultra-high-dimensional settings (Okolie et al., 2025, 2026). Ridge regularisation does not distort periodic signals like LASSO-type penalties that drive coefficients to zero. By dampening large fluctuations, ridge regularisation preserves the full contribution of Fourier terms (Savini, 2023; Kordani et al., 2025; Taiwo et al., 2026). Ridge penalisation is thus particularly well suited to climatic time series exhibiting persistent cyclic behaviour with multiple seasonal frequencies.

This study proposes a ridge-penalised Fourier autoregressive (PFAR-Ridge) framework. It fits tropical climatic time series. Further, the framework provides good forecast capabilities. The method uses harmonic representations for seasonality and ridge regularisation to achieve robust and interpretable estimation in high-dimensional periodic setups. The model is applied to monthly rainfall and relative humidity data, two atmospheric variables which show a high degree of persistence and changing periodicity in the tropics. Both in-sample and out-of-sample performance measures as well as residual diagnostics and parameter behaviour are used for evaluation. The current study's framework provides a robust alternative to classical ARIMA-type models for analysing complex seasonal dynamics in climatic time series. It provides a natural extension of the traditional FAR formulations through structured regularisation.

2. Materials and Methods

This section presents the methods that were used to model periodic time series with the FAR and ridge-penalised FAR (Ridge-PFAR) models. The procedure follows a structured series of stationarity test, model identification, parameter estimation, diagnostic checking, forecasting and performance evaluation. There are detailed procedures to ensure statistical validity, numerical stability and reliable out-sample predictive performance.

2.1 Stationarity Evaluation

The theoretical properties of FAR and Ridge-PFAR processes depend on the stationarity of the series. Stationarity is an essential property for autoregressive and Fourier-based models. Before we identify model and estimate, the stochastic properties of the series are examined to determine stationary or transformation is required.

Two complementary tests are used to assess stationarity, namely, the Augmented Dickey–Fuller (ADF) test and the Kwiatkowski–Phillips–Schmidt–Shin (KPSS) test. Each of them has a different null hypothesis and together they serve to reduce the chance of false conclusions.

2.1.1 Augmented Dickey–Fuller (ADF) test

The null hypothesis of ADF test is non-stationarity, which means presence of unit root in the time series. The additional regression is given by

$$\Delta y_t = \alpha + \gamma y_{t-1} + \sum_{i=1}^{k} \delta_i \, \Delta y_{t-i} + \varepsilon_t, \tag{1}$$

where $\Delta y_t = y_t - y_{t-1}$, $k$is the number of lagged differences, and $\varepsilon_t$is a white-noise error term.

The hypotheses are

$$H_0: \gamma = 0(\text{non-stationary}), H_1: \gamma < 0(\text{stationary}).$$

Rejection of H_0indicates stationarity of the series.

2.1.2 Kwiatkowski–Phillips–Schmidt–Shin (KPSS) test

The KPSS test complements the ADF test by assuming stationarity under the null hypothesis. The series is decomposed as

$$y_t = \mu_t + r_t + \varepsilon_t, \tag{2}$$

where $r_t = r_{t-1} + u_t$represents a random walk component.

The KPSS statistic is defined as

$$\text{KPSS} = \frac{\frac{1}{T^2}\sum_{t=1}^{T} S_t^2}{\hat{\sigma}^2}, S_t = \sum_{i=1}^{t} \hat{\varepsilon}_i, \tag{3}$$

with $\hat{\sigma}^2$denoting the long-run variance estimator.

The joint use of ADF and KPSS tests provides a robust stationarity assessment by exploiting their opposing null hypotheses.

2.2 Model Identification Using Periodic Autocorrelation Functions

Having established the stationarity, the next step is to identify the autoregressive order appropriate for the FAR framework. Due to the dependence structure being not constant by season, classical tools based on autocorrelation are not appropriate. Periodic extensions are thus used.

2.2.1 Periodic Autocorrelation Function (pACF)

For a periodic stationary process with period Ω, the periodic autocovariance at season τ and lag k is

$$\gamma_\tau(k) = \mathrm{Cov}(y_{m\Omega+\tau}, y_{m\Omega+\tau-k}), \tag{4}$$

and the periodic autocorrelation function is

$$\rho_\tau(k) = \frac{\gamma_\tau(k)}{\gamma_\tau(0)}. \tag{5}$$

Sample estimates are obtained using seasonal means and repeated cycles.

2.2.2 Periodic Partial Autocorrelation Function (pPACF)

The periodic partial autocorrelation function, denoted $\phi_{\tau\tau}(k)$, measures the direct dependence between periodic observations at lag $k$after removing intermediate effects. It is computed recursively as

$$\hat{\phi}_{\tau\tau}(k) = \frac{\hat{\gamma}_\tau(k) - \sum_{j=1}^{k-1} \hat{\phi}_{\tau\tau}(j)\hat{\gamma}_\tau(k-j)}{\hat{\gamma}_\tau(0) - \sum_{j=1}^{k-1} \hat{\phi}_{\tau\tau}(j)\hat{\gamma}_\tau(j)}. \tag{6}$$

The autoregressive order $p(\tau)$ is selected as the lag beyond which the pPACF becomes statistically insignificant.

2.3 Model specification

Let $\{y_t\}$ be a univariate periodic time series with fundamental period Ω. Write the time index as $t = m\Omega + \tau,\ \tau = 1, \dots, \Omega,\ m = 0,1, \dots$

where τ denotes the seasonal position within the cycle and m the cycle index.

The Fourier Autoregressive model of order $p(\tau)$ is defined as

$$y_{m\Omega+\tau} = \phi_0 + \sum_{j=1}^{p(\tau)} \left[\phi_j(\tau)\cos\left(\frac{2\pi m}{\Omega}\right) + \phi_j^*(\tau)\sin\left(\frac{2\pi m}{\Omega}\right)\right] y_{m\Omega+\tau-j} + \eta_{m\Omega+\tau}, \tag{7}$$

where ϕ_0 is a constant term, $\phi_j(\tau)$ and $\phi_j^*(\tau)$ are season-dependent Fourier autoregressive coefficients, and $\eta_{m\Omega+\tau}$ is a zero-mean white-noise process with periodic variance.

Define

$$\alpha_m = \cos\cos\left(\frac{2\pi m}{\Omega}\right),\ \ \beta_m = \sin\cos\left(\frac{2\pi m}{\Omega}\right).$$

Then Eq. (7) can be written more compactly as

$$y_t = \phi_0 + \sum_{j=1}^{p(\tau)} (\phi_j(\tau)\alpha_m + \phi_j^*(\tau)\beta_m) y_{t-j} + \eta_t, \quad t = m\Omega + \tau. \tag{8}$$

2.3.1 OLS estimation of the FAR model

For $t = 1, \dots, n$, making η_t in Eq. (8) the subject of formula, we have;

$$\eta_t = y_t - \phi_0 - \sum_{j=1}^{p(\tau)} (\phi_j(\tau)\alpha_m + \phi_j^*(\tau)\beta_m) y_{t-j}. \tag{9}$$

The ordinary least squares estimator is obtained by minimising the residual sum of squares

$$\mathrm{RSS_{FAR}} = \sum_{t=1}^{n} \eta_t^2$$
$$= \sum_{t=1}^{n} (y_t - \phi_0 - \phi_1 \alpha_m y_{t-1} - \phi_1^* \beta_m y_{t-1} - \cdots - \phi_p \alpha_m y_{t-p} - \phi_p^* \beta_m y_{t-p})^2 . (10)$$

Differentiating (10) partially with respect to $(\phi_j)\ and\ (\phi_j^*)$ coefficients, setting it to zero and solve for the coefficients, we have

$$\begin{bmatrix} \sum y_t \\ \sum \alpha y_t y_{t-1} \\ \sum \beta y_t y_{t-1} \\ \sum \alpha y_t y_{t-2} \\ \sum \beta y_t y_{t-2} \\ \vdots \\ \sum \alpha y_t y_{t-p} \\ \sum \beta y_t y_{t-p} \end{bmatrix}$$

$$= \begin{bmatrix} n & \sum \alpha y_{t-1} & \sum \beta y_{t-1} & \sum \alpha y_{t-2} & \sum \beta y_{t-2} & \cdots & \sum \alpha y_{t-p} & \sum \beta y_{t-p} \\ \sum \alpha y_{t-1} & \sum (\alpha y_{t-1})^2 & \sum \alpha\beta y_{t-1}^2 & \sum \alpha^2 y_{t-1} y_{t-2} & \sum \alpha\beta y_{t-1} y_{t-2} & \cdots & \sum \alpha^2 y_{t-1} y_{t-p} & \sum \alpha\beta y_{t-1} y_{t-p} \\ \sum \beta y_{t-1} & \sum \beta\alpha y_{t-1}^2 & \sum (\beta y_{t-1})^2 & \sum \beta\alpha y_{t-1} y_{t-2} & \sum \beta^2 y_{t-1} y_{t-2} & \cdots & \sum \beta\alpha y_{t-1} y_{t-p} & \sum \beta^2 y_{t-1} y_{t-p} \\ \sum \alpha y_{t-1} & \sum \alpha^2 y_{t-1} y_{t-2} & \sum \alpha\beta y_{t-1} y_{t-2} & \sum (\alpha y_{t-2})^2 & \sum \alpha\beta y_{t-2}^2 & \cdots & \sum \alpha^2 y_{t-2} y_{t-p} & \sum \alpha\beta y_{t-2} y_{t-p} \\ \sum \beta y_{t-2} & \sum \alpha\beta y_{t-1} y_{t-2} & \sum \beta^2 y_{t-1} y_{t-2} & \sum \alpha\beta y_{t-1}^2 & \sum (\beta y_{t-2})^2 & \cdots & \sum \alpha\beta y_{t-2} y_{t-p} & \sum \beta^2 y_{t-2} y_{t-p} \\ \vdots & \vdots & \vdots & \vdots & \vdots & \vdots & \vdots & \vdots \\ \sum \alpha y_{t-p} & \sum \alpha^2 y_{t-1} y_{t-p} & \sum \alpha\beta y_{t-1} y_{t-p} & \sum \alpha^2 y_{t-2} y_{t-p} & \sum \alpha\beta y_{t-2} y_{t-p} & \cdots & \sum (\alpha y_{t-p})^2 & \sum \alpha\beta y_{t-p}^2 \\ \sum \beta y_{t-p} & \sum \alpha\beta y_{t-1} y_{t-p} & \sum \beta^2 y_{t-2} y_{t-p} & \sum \alpha\beta y_{t-2} y_{t-p} & \sum \beta^2 y_{t-2} y_{t-p} & \cdots & \sum \alpha\beta y_{t-p}^2 & \sum (\beta y_{t-p})^2 \end{bmatrix}$$

$$\times \begin{bmatrix} \hat{\phi}_0 \\ \hat{\phi}_1 \\ \hat{\phi}_1^* \\ \hat{\phi}_2 \\ \hat{\phi}_2^* \\ \vdots \\ \hat{\phi}_p \\ \hat{\phi}_p^* \end{bmatrix} \quad (11)$$

Transforming (11) gives to matrix form gives;

$$\hat{\phi}_{FAR}^{OLS} = (Z'Z)^{-1}Z'Y, \tag{12}$$

where $Z'Y = \begin{bmatrix} \sum y_t \\ \sum \alpha y_t y_{t-1} \\ \sum \beta y_t y_{t-1} \\ \sum \alpha y_t y_{t-2} \\ \sum \beta y_t y_{t-2} \\ \vdots \\ \sum \alpha y_t y_{t-p} \\ \sum \beta y_t y_{t-p} \end{bmatrix}$, $\hat{\phi} = \begin{bmatrix} \hat{\phi}_0 \\ \hat{\phi}_1 \\ \hat{\phi}_1^* \\ \hat{\phi}_2 \\ \hat{\phi}_2^* \\ \vdots \\ \hat{\phi}_p \\ \hat{\phi}_p^* \end{bmatrix}$, $Z'Z$ is nonsingular and

$$Z'Z = \begin{bmatrix} n & \sum \alpha y_{t-1} & \sum \beta y_{t-1} & \sum \alpha y_{t-2} & \sum \beta y_{t-2} & \cdots & \sum \alpha y_{t-p} & \sum \beta y_{t-p} \\ \sum \alpha y_{t-1} & \sum (\alpha y_{t-1})^2 & \sum \alpha\beta y_{t-1}^2 & \sum \alpha^2 y_{t-1}y_{t-2} & \sum \alpha\beta y_{t-1}y_{t-2} & \cdots & \sum \alpha^2 y_{t-1}y_{t-p} & \sum \alpha\beta y_{t-1}y_{t-p} \\ \sum \beta y_{t-1} & \sum \beta\alpha y_{t-1}^2 & \sum (\beta y_{t-1})^2 & \sum \beta\alpha y_{t-1}y_{t-2} & \sum \beta^2 y_{t-1}y_{t-2} & \cdots & \sum \beta\alpha y_{t-1}y_{t-p} & \sum \beta^2 y_{t-1}y_{t-p} \\ \sum \alpha y_{t-1} & \sum \alpha^2 y_{t-1}y_{t-2} & \sum \alpha\beta y_{t-1}y_{t-2} & \sum (\alpha y_{t-2})^2 & \sum \alpha\beta y_{t-2}^2 & \cdots & \sum \alpha^2 y_{t-2}y_{t-p} & \sum \alpha\beta y_{t-2}y_{t-p} \\ \sum \beta y_{t-2} & \sum \alpha\beta y_{t-1}y_{t-2} & \sum \beta^2 y_{t-1}y_{t-2} & \sum \alpha\beta y_{t-1}^2 & \sum (\beta y_{t-2})^2 & \cdots & \sum \alpha\beta y_{t-2}y_{t-p} & \sum \beta^2 y_{t-2}y_{t-p} \\ \vdots & \vdots & \vdots & \vdots & \vdots & \ddots & \vdots & \vdots \\ \sum \alpha y_{t-p} & \sum \alpha^2 y_{t-1}y_{t-p} & \sum \alpha\beta y_{t-1}y_{t-p} & \sum \alpha^2 y_{t-2}y_{t-p} & \sum \alpha\beta y_{t-2}y_{t-p} & \cdots & \sum (\alpha y_{t-p})^2 & \sum \alpha\beta y_{t-p}^2 \\ \sum \beta y_{t-p} & \sum \alpha\beta y_{t-1}y_{t-p} & \sum \beta^2 y_{t-2}y_{t-p} & \sum \alpha\beta y_{t-2}y_{t-p} & \sum \beta^2 y_{t-2}y_{t-p} & \cdots & \sum \alpha\beta y_{t-p}^2 & \sum (\beta y_{t-p})^2 \end{bmatrix}$$

Given the identified order $p(\tau)$, parameters of the FAR model are estimated using ordinary least squares (OLS) and ridge penalisation.

2.3.2 Ridge-PFAR estimation

To stabilise estimation in high-dimensional periodic settings, improve generalization and reduce overfitting, ridge penalisation is introduced in Eq. (10). The penalised criterion is

$$RSS_{Ridge} = \sum_{i=1}^{n} \big(y_t - \phi_0 - \phi_1 \alpha y_{t-1} - \phi_1^* \beta y_{t-1} - \phi_2 \alpha y_{t-2} - \phi_2^* \beta y_{t-2} - \cdots - \phi_p \alpha y_{t-p} - \phi_p^* \beta y_{t-p}\big)^2 + \lambda_2 \sum_{j=1}^{p} \left((\phi_j)^2 + (\phi_j^*)^2 \right) \tag{13}$$

Also, we differentiating (13) partially with respect to (ϕ_j) and (ϕ_j^*) coefficients, setting it to zero and solve for the coefficients, we have

$$\begin{bmatrix} \sum y_t \\ \sum \alpha y_t y_{t-1} \\ \sum \beta y_t y_{t-1} \\ \vdots \\ \sum \alpha y_t y_{t-p} \\ \sum \beta y_t y_{t-p} \end{bmatrix}$$

$$= \begin{bmatrix} n & \sum \alpha y_{t-1} & \sum \beta y_{t-1} & \cdots & \sum \alpha y_{t-p} & \sum \beta y_{t-p} \\ \sum \alpha y_{t-1} & \sum (\alpha y_{t-1})^2 + \lambda_2 & \sum \alpha\beta y_{t-1}^2 & \cdots & \sum \alpha^2 y_{t-1} y_{t-p} & \sum \alpha\beta y_{t-1} y_{t-p} \\ \sum \beta y_{t-1} & \sum \beta\alpha y_{t-1}^2 & \sum (\beta y_{t-1})^2 + \lambda_2 & \cdots & \sum \beta\alpha y_{t-1} y_{t-p} & \sum \beta^2 y_{t-1} y_{t-p} \\ \vdots & \vdots & \vdots & \ddots & \vdots & \vdots \\ \sum \alpha y_{t-p} & \sum \alpha^2 y_{t-1} y_{t-p} & \sum \alpha\beta y_{t-1} y_{t-p} & \cdots & \sum (\alpha y_{t-p})^2 + \lambda_2 & \sum \alpha\beta y_{t-p}^2 \\ \sum \beta y_{t-p} & \sum \alpha\beta y_{t-1} y_{t-p} & \sum \beta^2 y_{t-2} y_{t-p} & \cdots & \sum \alpha\beta y_{t-p}^2 & \sum (\beta y_{t-p})^2 + \lambda_2 \end{bmatrix}$$

$$\times \begin{bmatrix} \hat{\phi}_0 \\ \hat{\phi}_1 \\ \hat{\phi}_1^* \\ \vdots \\ \hat{\phi}_p \\ \hat{\phi}_p^* \end{bmatrix} \qquad (14)$$

A transformation of (14) gives

$$\hat{\phi}_{FAR}^{Ridge} = (Z'Z + \Lambda_2)^{-1} Z'Y, \qquad (15)$$

where $\Lambda = diag(0, \lambda_2 I_{2p})$, I_{2p} is the identity on the $2p$ slope coefficients $(\phi_1, \phi_1^*, \dots, \phi_p, \phi_p^*)$.

with this,

$$\hat{\phi}_{FAR}^{Ridge} = (Z'Z + \Lambda_2)^{-1} Z'Y = \left(Z'Z + diag(0, \lambda_2 I_{2p})\right)^{-1} Z'Y \qquad (16)$$

$$Z'Y = \begin{bmatrix} \sum y_t \\ \sum \alpha y_t y_{t-1} \\ \sum \beta y_t y_{t-1} \\ \vdots \\ \sum \alpha y_t y_{t-p} \\ \sum \beta y_t y_{t-p} \end{bmatrix}; \quad \hat{\phi}_{Ridge} = \begin{bmatrix} \hat{\phi}_0 \\ \hat{\phi}_1 \\ \hat{\phi}_1^* \\ \vdots \\ \hat{\phi}_p \\ \hat{\phi}_p^* \end{bmatrix}; \text{ and}$$

$$Z'Z + diag(0, \lambda_2 I_{2p})$$

$$= \begin{bmatrix} n & \sum \alpha y_{t-1} & \sum \beta y_{t-1} & \cdots & \sum \alpha y_{t-p} & \sum \beta y_{t-p} \\ \sum \alpha y_{t-1} & \sum (\alpha y_{t-1})^2 + \lambda_2 & \sum \alpha\beta y_{t-1}^2 & \cdots & \sum \alpha^2 y_{t-1} y_{t-p} & \sum \alpha\beta y_{t-1} y_{t-p} \\ \sum \beta y_{t-1} & \sum \beta\alpha y_{t-1}^2 & \sum (\beta y_{t-1})^2 + \lambda_2 & \cdots & \sum \beta\alpha y_{t-1} y_{t-p} & \sum \beta^2 y_{t-1} y_{t-p} \\ \vdots & \vdots & \vdots & \ddots & \vdots & \vdots \\ \sum \alpha y_{t-p} & \sum \alpha^2 y_{t-1} y_{t-p} & \sum \alpha\beta y_{t-1} y_{t-p} & \cdots & \sum (\alpha y_{t-p})^2 + \lambda_2 & \sum \alpha\beta y_{t-p}^2 \\ \sum \beta y_{t-p} & \sum \alpha\beta y_{t-1} y_{t-p} & \sum \beta^2 y_{t-2} y_{t-p} & \cdots & \sum \alpha\beta y_{t-p}^2 & \sum (\beta y_{t-p})^2 + \lambda_2 \end{bmatrix}$$

2.4 Model Diagnostic

Once the model parameters have been estimated, it is important to check whether the Fourier Autoregressive (FAR) model is a good (adequate) model or not. The key assumption is that ε_t are white noise. We performed a detailed analysis of the residuals. The residuals' sample autocorrelation function (ACF) was calculated to check for any patterns. The residuals were statistically insignificant within two standard deviations at the $\alpha = 0.05$ level, meaning they are white noise and the specification is adequate.

2.5 Model Diagnostic

Given the Fourier Autoregressive model of order p, defined in equation (7) as

$$y_{m\Omega+\tau} = \phi_0 + \sum_{j=1}^{p(\tau)} \left\{ \phi_j(\tau) \cos\left(\frac{2\pi m}{\Omega}\right) + \phi_j^*(\tau) \sin\left(\frac{2\pi m}{\Omega}\right) \right\} y_{m\Omega+\tau-j} + \eta_{m\Omega+\tau},$$

where $y_{m\Omega+\tau}$ denotes the observation at time $m\Omega + \tau$, $\tau = 1,2, \ldots, \Omega$ is the seasonal index, and m represents the year index, forecasting in the FAR framework is based on recursively projecting future values using the estimated Fourier coefficients.

For a one-step-ahead forecast, the model can be expressed as

$$\hat{y}_{m\Omega+\tau}(1) = \hat{\phi}_0 + \sum_{j=1}^{p(\tau)} \left\{ \hat{\phi}_j(\tau) \cos\left(\frac{2\pi m}{\Omega}\right) + \hat{\phi}_j^*(\tau) \sin\left(\frac{2\pi m}{\Omega}\right) \right\} y_{m\Omega+\tau-j}. \quad (17)$$

Similarly, for an l-step-ahead forecast, the recursive equation becomes

$$\hat{y}_{m\Omega+\tau}(l) = \hat{\phi}_0 + \sum_{j=1}^{p(\tau)} \left\{ \hat{\phi}_j(\tau)\cos\left(\frac{2\pi m}{\Omega}\right) + \hat{\phi}_j^*(\tau)\sin\left(\frac{2\pi m}{\Omega}\right) \right\} \hat{y}_{m\Omega+\tau-}\ (l-1), \quad l \geq 1. \tag{18}$$

In this setup, the forecast at horizon l depends on previously forecasted values for $l-1$, making the process iterative. The periodic coefficients $\hat{\phi}_j(\tau)$ and $\hat{\phi}_j^*(\tau)$ capture both the amplitude and phase variations across seasons, allowing the FAR model to adapt dynamically to cyclic patterns in the data. This formulation enables efficient prediction of periodic and quasi-periodic time series, particularly in contexts such as climatology, finance, and environmental monitoring where seasonal fluctuations are pronounced.

2.5 Forecast Performance

While information criteria assess in-sample performance, forecast accuracy metrics are used to evaluate out-of-sample predictive behaviour.

Let y_t denote the observed value and $\hat{y}_t$ the corresponding forecast at time t, for $t = 1, \dots, n$.

2.5.1 Root Mean Square Error (RMSE)

The RMSE measures the average size of forecast errors, assigning greater penalty to larger deviations. It is defined as

$$\text{RMSE} = \sqrt{\frac{1}{n}\sum_{t=1}^{n}(y_t - \hat{y}_t)^2}. \tag{19}$$

Because RMSE is reported in the same units of measurement as the original series, it provides a straightforward and interpretable measure of forecast accuracy.

2.5.2 Mean Absolute Percentage Error (MAPE)

The MAPE is a measure of predictive accuracy of forecasting systems. Furthermore, it measures this in terms of percentage errors. For example, it is essentially the average of the absolute percentage errors. It is defined as

$$\text{MAPE} = \frac{100}{n}\sum_{t=1}^{n} \left| \frac{y_t - \hat{y}_t}{y_t} \right|. \tag{20}$$

Less MAPE means a more accurate forecast. However, the measurement must be viewed with prudence because of the observed values.

3. Results

This section presents the empirical results of the Fourier-based and penalised Fourier autoregressive models on climatic time series. The Nigerian Meteorological Agency (NIMET) provided monthly measurements of rainfall and relative humidity from 2014-2024 which are analyzed in order to assess the model's ability to capture seasonal and periodic dynamics. Analysis of the estimation of model selection and diagnostics are implemented in Python using the numerical routines from NumPy and scikit-learn. To evaluate the performance of the models in-sample information criteria and out-of-sample forecast accuracy measures were used. The findings from the research can be seen as supporting evidence for, or against, the benefit of ridge-penalisation in improving model stability and reducing overfitting and increasing predictive performance in climatic time series modelling.

According to Table 1, Nigeria's climate variables such as rainfall, relative humidity, solar radiation as well as wind speed have been presented in the descriptive statistics. The findings reveal how these variables generally behaved throughout the period studied, how they varied, and how they were distributed.

Relative humidity average value in Nigeria over the years is about 75.01 with a standard deviation value of about 10.99. This shows that relative humidity does not fluctuate that much from month to month. With minimum and maximum values of 39.0 and 88.0, respectively, it suggests the presence of high variability in the data due to seasonality. In particular, the difference between the dry and rainy seasons is most likely the cause. The negative skewness point which is -1.1240 indicates that higher humidities are frequent and the kurtosis value point which is 0.7304 indicates that the distribution is flatter than the normal distribution.

Essentially, it's the average amount of rain that is received in a month. The rainfall in the month of October has a mean of $99.62\ mm$ with a standard deviation of 95.21. The values range from 0.0 to $370.8\ mm$, showing the strong seasonal contrast between wet and dry months. A positive skewness of 0.6557 indicates that extreme rainfall is not uncommon, while a negative kurtosis of -0.5919 suggests a relatively flat distribution.

Table 4.1: Descriptive Statistics for Nigerian Monthly Rainfall, Humidity, GDP, and Inflation

Variable	Mean	Std. Dev.	Min	Max	Skewness	Kurtosis
Relative Humidity	75.0076	10.9986	39.0	88.0	-1.1240	0.7304
Rainfall	99.6174	95.2106	0.0	370.8	0.6557	-0.5919

Source: *Author's Computation*

As shown in Figure 1 and Figure 2, it has been confirmed that the rainfall and relative humidity series have strong periodic movements with peaks during the wet periods and troughs during the dry season. The amplitude of these seasonal fluctuations varies from year to year in both figures, suggesting a notable interannual variability and the occurrences of occasional extremes. Thus, it is not a stable deterministic cycle. The characteristics we outlined above create an interest in adopting modelling frameworks that capture temporal dependence with time-varying periodic behaviour. This underpins the use of Fourier-based and penalised autoregressive models in this paper.

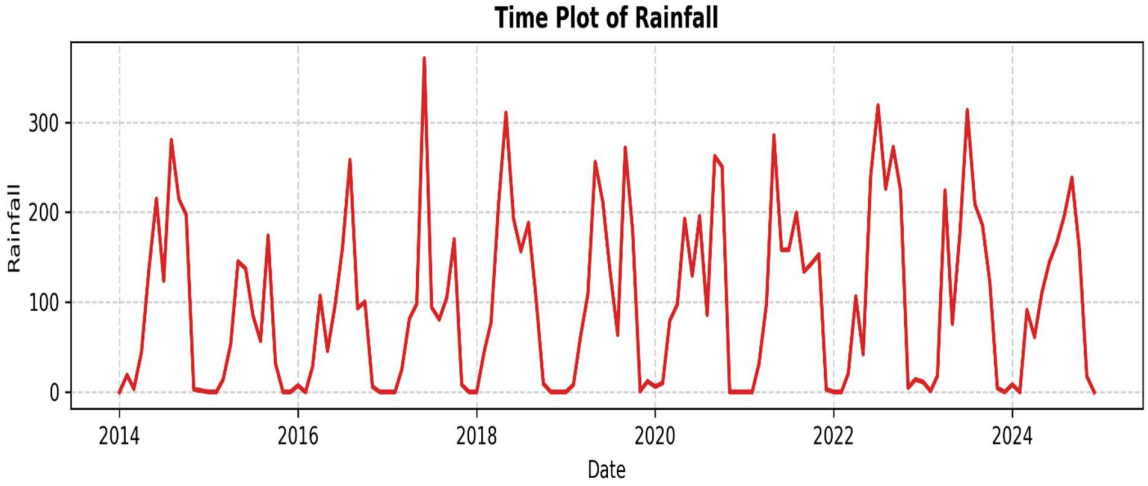


Figure 1: Monthly Rainfall in Nigeria (2014–2024)

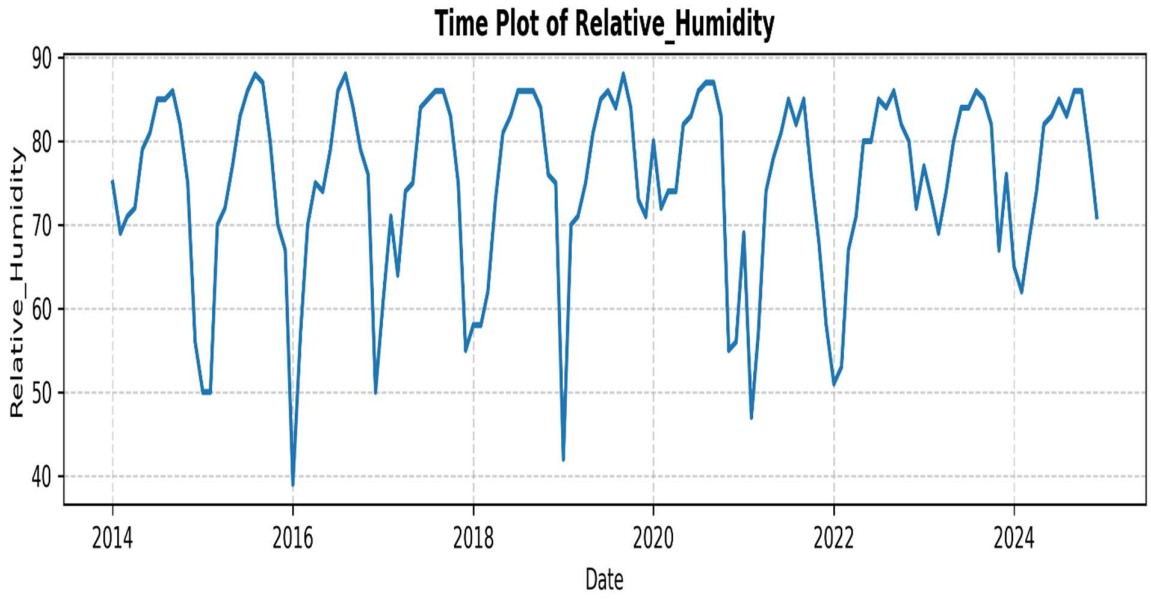


Figure 2: Monthly Humidity in Nigeria (2014–2024)

The stationarity test results for rainfall and relative humidity are given in Table 2 based on the ADF and KPSS procedures. Both series are non-stationary at levels as seen from the insignificant ADF statistics and the KPSS statistics that do not support stationarity. After first differencing, the ADF test strongly rejects the unit root hypothesis while the KPSS test fails to reject stationarity for both variables. This means that rainfall and relative humidity become stationary at first differencing which is suitable for modelling.

Table 2: Stationarity Tests (ADF and KPSS)

Difference	Variable	ADF Statistic	ADF p-value	KPSS Statistic	KPSS p-value	Decision
0	Humidity	-2.4444	0.1296	0.0746	0.1000	Non-Stationary
0	Rainfall	-1.8846	0.3393	0.1449	0.1000	Non-Stationary
1	Humidity	-10.6882	0.0000	0.0125	0.1000	Stationary
1	Rainfall	-8.6017	0.0000	0.0368	0.1000	Stationary

Source: *Author's Computation*

Table 3 shows AIC and BIC with respect to rainfall and relative humidity of in-sample model comparison. According to the study of rainfall, the best conventional integrated autoregressive model is $ARIMA(1,1,1)$ as it gave minimum $AIC = 1253.52$ and $BIC = 1261.54$. However, all Fourier-based models are obtained with much lower values. Further, $FAR(4, K = 2)$ gave the minimum $AIC = 1179.67$ and $BIC = 1203.39$.

A similar trend can be noted in respect of relative humidity, where the lowest ARIMA values ($AIC = 785.81$, $BIC = 799.17$ for $ARIMA(2,1,2)$) are surpassed by FAR models, with $FAR(4, K = 2)$ having an $AIC = 678.61$ and $BIC = 702.32$. Penalised ridge FAR models are close to the unpenalised model e.g. $PFAR(4)$-Ridge $AIC = 1179.94$ and $BIC = 1203.65$ for rainfall, $AIC = 679.52$ and $BIC = 703.23$ for relative humidity.

Table 3: In-sample Model Comparison Based on AIC and BIC for Rainfall and Relative Humidity

Model	Rainfall		Relative Humidity	
	AIC	BIC	AIC	BIC
$ARIMA(0,1,1)$	1271.58	1276.93	787.31	792.66
$ARIMA(0,1,2)$	1260.20	1268.22	789.23	797.25
$ARIMA(1,1,0)$	1272.40	1277.74	787.31	792.66
$ARIMA(1,1,1)$	1253.52	1261.54	789.30	797.32
$ARIMA(1,1,2)$	1275.52	1286.22	791.21	801.90
$ARIMA(2,1,0)$	1272.85	1280.87	789.26	797.28
$ARIMA(2,1,1)$	1254.95	1265.64	791.25	801.95
$ARIMA(2,1,2)$	1257.46	1270.83	785.81	799.17
$FAR(1,K=2)$	1234.53	1250.51	721.97	737.95
$FAR(2,K=2)$	1207.41	1225.98	697.62	716.20
$FAR(3,K=2)$	1188.26	1209.42	684.60	705.76
$FAR(4,K=2)$	1179.67	1203.39	678.61	702.32
$PFAR(1)-Ridge$	1234.64	1250.62	722.09	738.07
$PFAR(2)-Ridge$	1207.43	1226.01	697.71	716.29
$PFAR(3)-Ridge$	1188.34	1209.49	685.17	706.33
$PFAR(4)-Ridge$	1179.94	1203.65	679.52	703.23

Source: *Author's Computation*

Table 4 summarizes the out-of-sample forecast accuracy of competing models using RMSE and MAPE for rainfall and relative humidity. The $ARIMA(1,1,1)$ model for rainfall records high forecast errors ($RMSE = 90.94,\ MAPE = 515.34$) while Fourier-based models show considerable improvements with FAR(4) lowering the RMSE to 73.72 and $PFAR(4)$-Ridge who performed the best with the lowest RMSE of 73.31 and MAPE of 197.09. Similar pattern was observed in relative humidity as $ARIMA(2,1,2)$ with $RMSE = 9.68$ and $MAPE = 10.62$. $FAR(4)$ and $PFAR(4)$-Ridge gives RMSE of 6.60 and 6.34, respectively. The results show that the Fourier-based models outperform standard integraed autoregressive models while ridge penalisation gives extra forecast improvement.

Rainfall and Humidity Diagnostic results for PFAR-Ridge in Figure 3 and 4 presented. As illustrated in Figure 3, the residuals oscillate consistently about zero and do not follow a given pattern, indicating that the model has successfully captured the periodic structure in the rainfall series. The residual ACF shows that nearly all autocorrelations stay within the confidence bounds. The histogram and the QQ plot indicate that the normality is approximately there (with slight tail deviation). Thus, the PFAR–Ridge suffices verification.

The residuals in figure 4 appears to be well behaved and have no strong serial dependence remaining after fitting the relevant model. The residual distribution is fairly symmetric, and the QQ plot is close to the theoretical normal line except for small deviations at the tails. Thus, we can say the PFAR–Ridge model is a good fit for the humidity series.

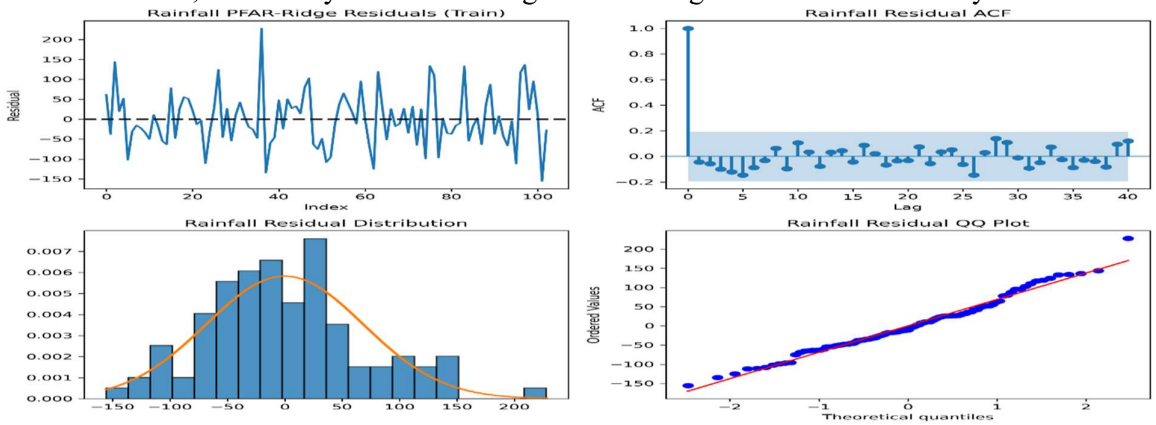


Figure 3: Diagnostic Plots for Rainfall under the $PFAR$(Ridge) Model

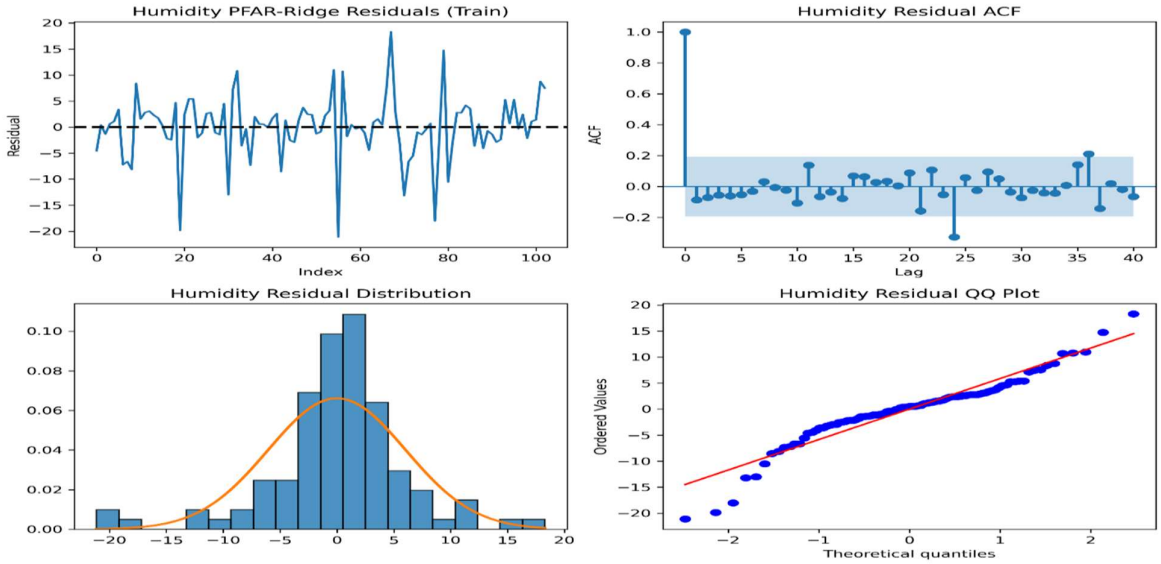


Figure 4: Diagnostic Plots for Humidity under the PFAR(Ridge) Model

According to Table 4, out-of-sample performance results of various models of rainfall and relative humidity using RMSE and MAPE. The classic $ARIMA(1,1,1)$ model gives quite high forecast errors for rainfall ($RMSE = 90.94$; $MAPE = 515.34$). In contrast, the Fourier-based models bring about significant improvements. For one, $FAR(4)$ reduces the errors to $RMSE = 73.72$. Similarly, $PFAR(4)$-Ridge provides the least errors ($RMSE = 73.31$; $MAPE = 197.09$). Relative humidity experiences the same behavior, with $ARIMA(2,1,2)$ yielding a greater forecast error ($RMSE = 9.68$; $MAPE = 10.62$) than $FAR(4)$ ($RMSE = 6.60$) and $PFAR(4)$-Ridge ($RMSE = 6.34$). The findings suggest that the use of Fourier terms substantially improves accuracy, while ridge penalisation further enhances results through improved generalisation performance, particularly with strong periodic dynamics in the data.

Table 4: Forecast Performance Metrics for Rainfall and Humidity Models

Variable	Model	RMSE	MAPE (%)
Rainfall	$ARIMA(1,1,1)$	90.94	515.34
	$FAR(4)$	73.72	202.01
	$PFAR(4) - Ridge$	73.31	197.09
Humidity	$ARIMA(2,1,2)$	9.6767	10.6170
	$FAR(4)$	6.5984	100.9510
	$PFAR(4) - Ridge$	6.3425	96.9757

Source: *Author's Computation*

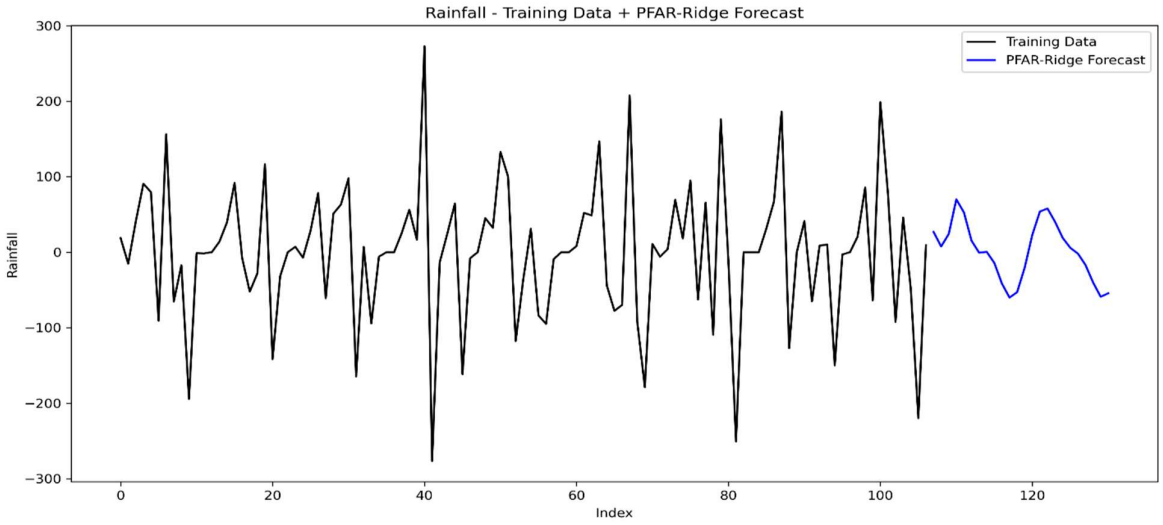


Figure 4.5: Forecast Plot for PFAR(4) −Ridge for Rainfall

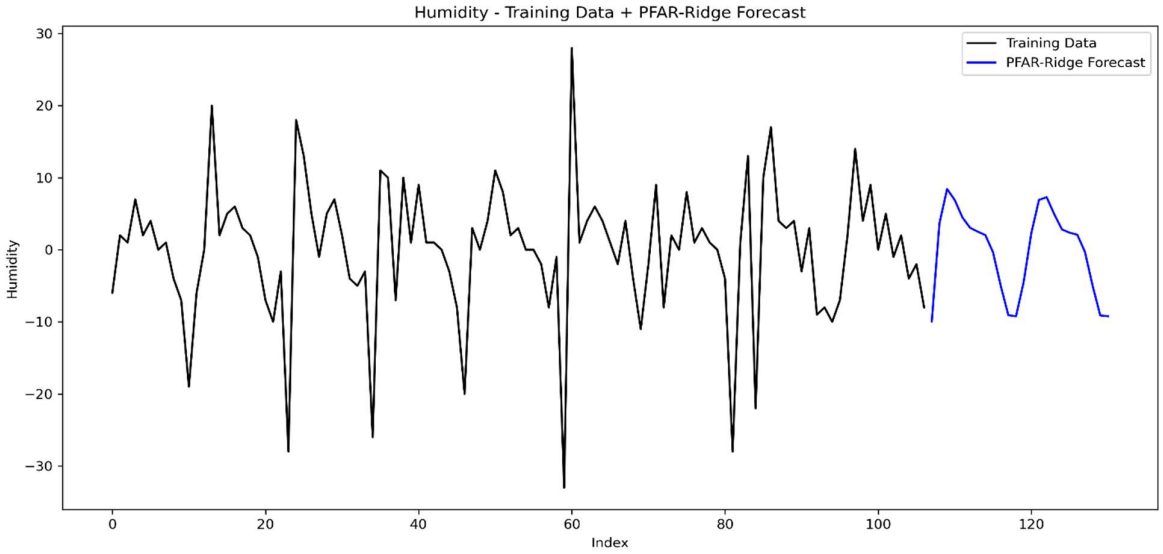


Figure 4.6: Forecast Plot for PFAR(4) − Ridge for Relative humidity

4. Discussion

This study is aimed to evaluate the effectiveness of the Fourier based and ridge-penalised Fourier autoregressive models that capture the pronounced periodic and persistent nature of tropical climatic time series, especially the rainfall and relative humidity. The empirical evidence is highly consistent with the theoretical motivations presented in the literature, and in addition, shows that structured regularisation is beneficial in high-dimensional periodic situations.

As shown by previous studies in climatic times series, the exploratory analysis indicates that both rainfall and relative humidity are inherently seasonal, persistent and interannual. This is consistent with what has been reported for tropical areas. Such features echo findings found in (Gil-Alana *et al*., 2019) and (Jackson *et al*., 2025), who contend that tropical hydro-climatic variables are governed by dominant annual and semi-annual cycles, bearing superimposed persistent stochastic components. The modeling of such dynamics could pose challenges for

standard autoregressive models, which typically necessitate substantial differencing and/or stringent seasonal specifications.

Integrated autoregressive model observations corroborate limitations reported in in-sample model comparison results. The ARIMA specifications were able to get reasonable fits but the AIC and BIC values were purposedly greater than those of Fourier-based specifications. This finding supports previous work suggesting that ARIMA and SARIMA frameworks, while being effective for short-memory processes, cannot flexibly capture multifrequency seasonal behaviour without losing information or over-parameterising (Effrosynidis et al., 2023; Arumugan & Natarajan, 2023). On the other hand, the FAR models represented periodic structure in a more parsimonious fashion, leading to substantial information criteria improvements for both climate variables.

The better performance of the FAR models obtained in the present study agrees with the findings of (Taiwo et al., 2019; Taiwo et al.,2020), who argued that Fourier autoregressive formulations perform better than classical autoregressive and integrated models with respect to preserving smooth seasonal effects and more stable periodic forecasts. However, those studies relied mostly on discrete Fourier transform–based estimation without any explicit regularisation, the present results show an important extension. With an increasing autoregressive order and a larger number of harmonics, the unpenalised FAR models are prone to overfitting and multicollinearity, as pointed out by (Papaioannou et al., 2022; Savini, 2023). Ridge penalisation introduction shuns this complication. The PFAR-Ridge model obtained information criterion values that are similar, and in some cases slightly larger, than the corresponding values for the unpenalised FAR model, but with better out-of-sample forecast accuracy. This behaviour is in line with what is expected from ridge regularisation theory, as it reduces the size of the coefficient but does not eliminate harmonic components, thereby stabilising estimation and maintaining the smooth periodicity property of the series (Kordani et al., 2025). Ridge penalisation does not induce spurious discontinuities in the seasonal patterns of rainfall and humidity forecasts unlike LASSO-type penalties which drive some Fourier coefficients to zero.

This conclusion is further reinforced by out-of-sample forecasting results. The significant drop in RMSE and MAPE values shown by PFAR–Ridge as compared to ARIMA and unpenalised FAR shows that its generalisation performance is improved. According to large-scale comparative studies, environmental forecasting problems are best solved using regularised regression-based approaches as opposed to classical time series models. The findings also show that the data has robust persistence and complex seasonal behaviour (Effrosynidis et al., 2023). The PFAR–Ridge model also exhibits the ideal forecasting characteristics seen in the earlier rainfall studies utilizing FAR models through the generation of continuous and stable period forecasts, but applicable to more complex and high-dimensional scenarios.

Residual diagnostics provide additional evidence of model adequacy. The diagnostics of PFAR–Ridge provide evidence for the fitted model's ability to capture the autoregressive dependence and seasonal structure as the significant residual autocorrelations are absent and normality is approximately satisfied. The outcome of this research is in line with the previous FAR diagnostics as discussed in the work of (Taiwo et al., 2019) and (Taiwo et al.,2020). However, unlike these previous works the results in the current work are more stable due to penalisation. The enhancement in residual behaviour provides further support for the contention that ridge-penalised Fourier autoregressive models represent a statistically robust and practically viable alternative to more conventional approaches for analysis of climatic time series.

The results of this research integrate FAR modelling from earlier times with more modern-day regularisation. The PFAR-Ridge framework that integrates Fourier-based seasonal

representation with ridge penalisation extends the current methodologies for overfitting and multicollinearity problems and evolving dynamics that are common in tropical climate time series. The findings not only reinforce previous empirical evidence but also contribute new insights into how structured regularisation in periodic time series forecasting works.

5. Conclusion

The study proves that Fourier-based representation with ridge penalisation provide a robust and flexible model for forecasting climatic time series with strong seasonality, persistence and changing periodic dynamics. Fourier autoregressive models dramatically outperform standard integrated autoregressive specifications due to their enhanced seasonal structure. Additionally, the introduction of ridge penalisation (or some other regularisation process) positively contributes to numerical stability and out-of-sample forecasting performance. Evidently, the PFAR–Ridge model produces well-behaved residuals which satisfy key statistical adequacy conditions. Forecast evaluations show a consistent gain over an unpenalised Fourier model as well as a benchmark classical model. In the context of analysis of climatic time series, the results highlight the value of structured regularisation for extending Fourier based autoregressive (AR) models to high dimensional noise-rich settings, offering a principled and effective alternative for modelling and forecasting periodic time series.

Reference

[1]. Arumugam, V., & Natarajan, V. (2023). Time series modeling and forecasting using autoregressive integrated moving average and seasonal autoregressive integrated moving average models. Instrumentation, Mesures, Métrologies, 22(4). https://doi.org/10.18280/i2m.220404

[2]. Borma, L. S., Costa, M. H., da Rocha, H. R., Arieira, J., Nascimento, N. C. C., Jaramillo-Giraldo, C., ... & Nobre, C. A. (2022). Beyond carbon: The contributions of South American tropical humid and subhumid forests to ecosystem services. Reviews of Geophysics, 60(4), e2021RG000766. https://doi.org/10.1029/2021RG000766

[3]. Effrosynidis, D., Spiliotis, E., Sylaios, G., & Arampatzis, A. (2023). Time series and regression methods for univariate environmental forecasting: An empirical evaluation. Science of The Total Environment, 875, 162580. https://doi.org/10.1016/j.scitotenv.2023.162580

[4]. El Zein, A. L., & Chehayeb, N. A. (2015). The effect of greenhouse gases on Earth's temperature. International Journal of Environmental Monitoring and Analysis, 3(2), 74. https://doi.org/10.11648/j.ijema.20150302.16

[5]. Gevaudan, M. (2021). Influence of salinity on the coupled ocean-atmosphere dynamics of the tropical Atlantic Ocean (Doctoral dissertation, Université Paul Sabatier-Toulouse III).

[6]. Gil-Alana, L. A., Yaya, O. S., & Fagbamigbe, A. F. (2019). Time series analysis of quarterly rainfall and temperature (1900–2012) in sub-Saharan African countries. Theoretical and Applied Climatology, 137(1), 61–76. https://doi.org/10.1007/s00704-018-2583-5

[7]. Jackson, L. S., Birch, C. E., Chagnaud, G., Marsham, J. H., & Taylor, C. M. (2025). Daily rainfall variability controls humid heatwaves in the global tropics and subtropics. Nature Communications, 16(1), 3461. https://doi.org/10.1038/s41467-025-58694-6

[8]. Kordani, M., Bagheritabar, M., Ahmadianfar, I., & Samadi-Koucheksaraee, A. (2025). Forecasting water quality indices using generalized ridge model, regularized weighted kernel ridge model, and optimized multivariate variational mode decomposition. Scientific Reports, 15(1), 16313. https://doi.org/10.1038/s41598-025-99341-w

[9]. Makokha, J. W., Barasa, P. W., & Khamala, G. W. (2025). Enhancing climate resilience: A data-driven north rift weather prediction system for real-time forecasting and agricultural decision support. Heliyon, 11(4). https://doi.org/10.1016/j.heliyon.2025.e42549.

[10]. Met Office. (2024). Understanding humidity. Retrieved from Met Office: https://weather.metoffice.gov.uk/learn-about/weather/types-of-weather/humidity

[11]. Okolie, F. A., Akarawak, E. E. E., and Olufolabo, O. O. (2026). Penalized Cox Regression and Its Application to Microarray Survival Data. International Journal of Mathematical Sciences and Optimization: Theory and Applications, 12(1), 1-10. Retrieved from https://www.ajol.info/index.php/ijmso/article/view/336983

[12]. Okolie, F. A., Fagbemigun, B. O., Taiwo, O. E., and Adekola, E. O. (2025). Comparing Ordinary Least Squares, Ridge, and Lasso Regression for Multicollinearity Mitigation in Linear Models. International Journal of Mathematical Sciences and Optimization: Theory and Applications, 11(4), 46-56. doi:https://doi.org/10.5281/zenodo.18986070

[13]. Papaioannou, P. G., Talmon, R., Kevrekidis, I. G., & Siettos, C. (2022). Time-series forecasting using manifold learning, radial basis function interpolation, and geometric harmonics. Chaos: An Interdisciplinary Journal of Nonlinear Science, 32(8). https://doi.org/10.1063/5.0094887

[14]. Sartorius, J. V., Geddes, A., Gagnon, A. S., & Burnett, K. A. (2024). Participation and co-production in climate adaptation: Scope and limits identified from a meta-method review of research with European coastal communities. Wiley Interdisciplinary Reviews: Climate Change, 15(3), e880. https://doi.org/10.1002/wcc.880

[15]. SAVINI, F. (2023). Automatic wavelet-based seasonality estimator for non-stationary time series. Taiwo, A. I., Olatayo, T. O., & Agboluaje, S. A. (2020). Time series model building with Fourier autoregressive model. South African Statistical Journal, 54(2). https://doi.org/10.37920/sasj.2020.54.2.8

[16]. Taiwo, A. I., Okolie, F. A., & Olatayo, T. O. (2026). Ridge-Regularised Fourier Autoregression for periodic climate time series: Simulation evidence and an application to Nigerian rainfall and humidity. Journal of Applied Mathematics & Data Analytics, 2(2), 48–59.

[17]. Taiwo, A. I., Olatayo, T., Adedayo, A., & Adesanya, K. K. (2019). Modeling and forecasting periodic time series data with Fourier autoregressive model. Iraqi Journal of Science. https://doi.org/10.24996/ijs.2019.60.6.20

[18]. The British Geographer. (2014). The climate of tropical regions. Retrieved from https://thebritishgeographer.weebly.com/the-climate-of-tropical-regions.html

[19]. Zhou, S., Yu, B., Lintner, B. R., Findell, K. L., & Zhang, Y. (2023). Projected increase in global runoff dominated by land surface changes. Nature Climate Change, 13(5), 442–449. https://doi.org/10.1038/s41558-023-01659-8